Air bearing platforms for simulation of spacecraft attitude control systems

Alexandre Macedo de Oliveira[1], **Hélio Koiti Kuga**[1] **and Valdemir Carrara**[1]

[1]Instituto Nacional de Pesquisas Espaciais - Av. dos Astronautas, 1758, São José dos Campos, Brazil, CEP 12227-010
alexandre.oliveira@inpe.br, helio.kuga@inpe.br, valdemir.carrara@inpe.br

Abstract: This paper presents the development of two different air bearing tables, which can simulate attitude control systems for satellites with hardware-in-the-loop dynamics and control. Both systems are based on gas-bearing platforms in which several sensors and actuators were fixed. The first platform has a MEMS inertial sensor, and the second platform has several sensors and actuators that are engineering models similar to those usually employed in satellites. A PC/104 computer commands the first platform, which is responsible for driving 8 cold gas thrusters. On the other hand, the second platform is based on a Renesas 32 bits processor, which is responsible for three different subsystems: power supply, data handling and attitude control. The actuators in this case are reaction wheels and magnetic torque coils. The most important process for the correct operation of the simulators is to ensure accurate balancing of both platforms, because a difference between the center of gravity of the platform and the center of rotation of the bearing support may generate higher torques than those normally encountered in the space environment, invalidating the main feature of the simulator. Therefore, we use non-linear filtering to obtain the platforms mass properties, including the center of gravity position. Finally, we validate the mass properties by implementing two simple attitude stabilization controllers. Considerations on the nature of the friction of the two platforms will also be made in the end of this paper.

Keywords: air bearing, attitude control, satellite simulator, Kalman filter, inertial systems.

INTRODUCTION

Air bearing tables have been used for test and verification of software and embedded electronic for at least 50 years since the beginning of the space race (Schwartz et al., 2003). The idea behind an air bearing satellite simulator is to provide three-axis angular movement in a frictionless environment, similar to the outer space. It is known that this idealization is not valid since there are many disturbance torques on the system. Drag, bearing friction and gravity center offset are the major source of disturbance torques that must be modeled in order to validate the environment. They must be minimized until becoming compatible with the torque normally found in the space environment, ensuring the validity of simulators.

In the 1970s, research in air bearings were responsible for studies of internal energy dissipation effects in space platforms (sloshing, drive mechanisms and joints) because failures were detected in various missions. Although the technology has also been widely used by the Russians (Soviets) at the same time, little relevant information was found to complement the historical review from Schwartz et al. (2003).

To achieve the goal of studying different types of AOCS (Attitude and Orbit Control Systems) to meet the upcoming Brazilian missions, two types of different three-axis air-bearing tables were equipped with several sensors and actuators, with characteristics similar to the equipment that will be employed in those missions. A PC/104 computer commands the first platform, which is responsible for driving 8 cold gas thrusters. On the other hand, the second platform is based on a Renesas 32 bits processor, which is responsible for three different subsystems: power supply, data handling and attitude control. The actuators in this case are reaction wheels and magnetic torque coils. The most important process for the correct operation of the simulators is to ensure accurate balancing of both platforms, because a difference between the center of gravity of the platform and the center of rotation of the bearing support may generate higher torques than those normally encountered in the space environment, invalidating the main feature of the simulators.

This paper will be described as follows. First of all, a brief description of the attitude kinematics and dynamics of a rigid bod and a summary of nonlinear filtering concepts is presented, showing two methods: EKF and LSQ. Then the description of the two platforms and equipment is performed. Finally, one simple attitude control algorithm for each platform is presented, in order to validate the estimated parameters.

ATTITUDE KINEMATICS AND DYNAMICS

Attitude kinematics of a generic body can be described in different modes. Usually, Euler angles or quaternions are used. The use of quaternions is justified by computational facility, since trigonometric functions are avoided, circumventing computational problems like divisions by zero. On the other hand, it presents some difficulty for attitude estimation due to the lack of independence of the four quaternion components, wich are related by the constraint that the quaternion has unit module. This constraint results in the singularity of the covariance matrix of the quaternion state (Lefferts et al.,

1962). With this view, we will use Euler angles for attitude propagation. The body attitude with respect to the inertial reference can be represented by three separate rotations that align the two distinct reference systems. In the LVLH (Local Vertical, Local Horizontal) system (East(X)-North(Y)-Up(Z)), the motion around X-axis is called pitch (θ), around Y-axis is called roll (ϕ) and around Z-axis is called heading (ψ). The LVLH system will be considered inertial system in this paper. Hence, the rotation sequence used in this work for Euler angles is 3-2-1 (Hugues, 1986; Wertz, 1978), represented by the following transformation matrix $\mathbf{C}_{br}$:

$$\mathbf{C}_{br} = \begin{bmatrix} \cos\phi\cos\psi & \cos\phi\sin\psi & -\sin\phi \\ \sin\phi\sin\theta\cos\psi - \cos\phi\sin\psi & \sin\phi\sin\theta\sin\psi + \cos\phi\cos\psi & \sin\phi\cos\theta \\ \cos\phi\sin\theta\cos\psi + \sin\phi\sin\psi & \cos\phi\sin\theta\sin\psi - \sin\phi\cos\psi & \cos\phi\cos\theta \end{bmatrix}. \tag{1}$$

The set of kinematic equations are given by:

$$\begin{bmatrix} \dot{\phi} \\ \dot{\theta} \\ \dot{\psi} \end{bmatrix} = \begin{bmatrix} 1 & \sin\phi\tan\theta & \cos\phi\tan\theta \\ 0 & \cos\phi & -\sin\phi \\ 0 & \sin\phi/\cos\theta & \cos\phi/\cos\theta \end{bmatrix} \begin{bmatrix} \omega_x \\ \omega_y \\ \omega_z \end{bmatrix}, \tag{2}$$

where ω_x, ω_y and ω_z are the angular velocity components measured in the body reference system.

The attitude dynamics of a rigid body is defined by the angular momentum law with respect to an inertial frame $\dot{\mathbf{h}} = \mathbf{T}$, where $\mathbf{h}$ is the angular momentum vector, defined as $\mathbf{h} = \mathbf{I}\omega$, in which $\mathbf{I}$ is the body inertia matrix, ω is the body angular velocity vector, and $\mathbf{T}$ is the sum of external torques, divided into environmental and control torques, defined by $\mathbf{T} = \mathbf{T_{env}} + \mathbf{T_{con}}$. When expressed in a frame attached to the body, the attitude dynamics of a rigid body is represented by $\mathbf{I}\dot{\omega} + \omega \times \mathbf{I}\omega = \mathbf{T}$. Thus, the rigid body dynamics is a nonlinear function described in terms of angular velocities and external torque:

$$\dot{\omega} = \mathbf{I}^{-1}[\mathbf{T} - \omega \times \mathbf{I}\omega]. \tag{3}$$

The torque caused by the displacement of the center of gravity $\mathbf{T_{CG}}$ is obtained by:

$$\mathbf{T_{CG}} = \mathbf{R_{CG}} \times \mathbf{P}, \tag{4}$$
$$\mathbf{P} = [\,0 \ \ 0 \ \ -mg\,]^{\mathbf{T}}, \tag{5}$$

where $\mathbf{R_{CG}}$ is the the center of gravity position vector of the bearing with respect with the bearing rotation center and $\mathbf{P}$ is the weight vector. It can be noted that the vector $\mathbf{R_{CG}}$ is measured in body system reference and the vector $\mathbf{P}$ is known in the topocentric system reference, where m is the total mass of the table and g is the local gravity acceleration. As torque is applied to the rigid body, we need to transform its coordinates from the local reference system to the body reference system $\mathbf{T_{CG}} = \mathbf{R_{CG}} \times \mathbf{C_{br}P}$, where $\mathbf{C_{br}}$ is the rotation matrix defined in Eq. 1.

EXTENDED KALMAN FILTER

Kalman filter, in its standard form, is an optimal minimum variance linear estimator incorporating uncertainties in the dynamic and observation models. Unlike its linear version, the extended Kalman filter is not optimal due to truncation of higher order terms. Extended Kalman Filter is a state estimation algorithm that, with some adjustments, can also be used for parameter estimation. Most references on the subject divides the algorithm into two phases: prediction and correction (Aguirre, 2007; Maybeck, 1979, Gelb, 2001). We define a generic system with input vector $\mathbf{u}$, the state vector $\mathbf{x}$ and measurement vector $\mathbf{y}$, described by:

$$\dot{\mathbf{x}} = \mathbf{f}(\mathbf{x}, \mathbf{u}, t) + \mathbf{w_k}, \tag{6}$$
$$\mathbf{y_{k+1}} = \mathbf{h_{k+1}}(\mathbf{x_{k+1}}) + \mathbf{v_{k+1}}. \tag{7}$$

The functions $\mathbf{f}$ and $\mathbf{h_{k+1}}$ are nonlinear functions linking the state vector $\mathbf{x}$ to the dynamics and observation models, respectively. The process noise and observation noise are represented by random variables $\mathbf{w_k} = \mathbf{N}(\mathbf{0}, \mathbf{Q})$ and $\mathbf{v_k} = \mathbf{N}(\mathbf{0}, \mathbf{R})$, Gaussian distributions with zero mean and covariance $\mathbf{Q}$ and $\mathbf{R}$, in this sequence.

The first phase (prediction) of the EKF is based entirely on the dynamics of the system. Given the initial state vector $\mathbf{x_0}$ at time t_0, and knowing the input $\mathbf{u}$ applied over time, the system states can be propagated and therefore predicted in any time t_1, with $t_1 > t_0$. This propagation is therefore done via numerical integration of the Eq. 6 considering no uncertainty. For the covariance prediction, we use continuous Riccati equation that incorporates the uncertainty of each state equation of the model to the covariance matrix:

$$\dot{\mathbf{P}} = \mathbf{FP} + \mathbf{PF^T} + \mathbf{GQG^T}, \tag{8}$$

where $\mathbf{G}$ is the association matrix between the process noise and covariance matrix, and $\mathbf{F}$ is the Jacobian matrix of $\mathbf{f}$. The correction process is done by comparing the obtained measurement from the predicted state $\mathbf{x_{k+1}}$ with the actual

value of $\mathbf{y_{k+1}}$ obtained by the sensor at time t_1, with $t_1 > t_0$. The balance (weighing) between the predicted values and the values obtained by the sensors is given by the Kalman gain $\mathbf{K_{k+1}}$. Thus, the equations that summarize the correction process are:

$$\mathbf{K_{k+1}} = \bar{\mathbf{P}}_{\mathbf{k+1}}\mathbf{H}_{\mathbf{k+1}}^{\mathbf{T}}[\mathbf{H_{k+1}}\bar{\mathbf{P}}_{\mathbf{k+1}}\mathbf{H}_{\mathbf{k+1}}^{\mathbf{T}} + \mathbf{R_{k+1}}]^{-1} \tag{9}$$

$$\hat{\mathbf{P}}_{\mathbf{k+1}} = [\mathbf{I} - \mathbf{K_k}\mathbf{H_{k+1}}]\bar{\mathbf{P}}_{\mathbf{k+1}} \tag{10}$$

$$\mathbf{Res_{k+1}} = \mathbf{y_{k+1}} - \mathbf{h}(\bar{\mathbf{x}}_{\mathbf{k+1}}) \tag{11}$$

$$\hat{\mathbf{x}}_{\mathbf{k+1}} = \bar{\mathbf{x}}_{\mathbf{k+1}} + \mathbf{K_{k+1}}\mathbf{Res_{k+1}}, \tag{12}$$

where $\bar{\mathbf{P}}$ is the predicted covariance matrix and $\hat{\mathbf{P}}$ is the corrected covariance matrix. The vector $\hat{\mathbf{x}}_{\mathbf{k+1}}$ is the best estimate for the state at time $k + 1$. The residue $\mathbf{Res}$ is defined as the difference between the sensor measurement and the value of the nonlinear function $\mathbf{h}$ applied to $\bar{\mathbf{x}}_{\mathbf{k+1}}$. The matrix $\mathbf{H}$ is the Jacobian of $\mathbf{h}$, applied at the point $\bar{\mathbf{x}}_{\mathbf{k+1}}$.

NON-LINEAR LEAST SQUARES

We assume the following continuous-discrete dynamic system:

$$\dot{\mathbf{x}} = \mathbf{f}(\mathbf{x}, \mathbf{u}, t) \tag{13}$$

$$\mathbf{y_{k+1}} = \mathbf{h_k}(\mathbf{x_k}) + \mathbf{v_k} \tag{14}$$

Unlike the EKF, the system dynamics is considered perfect, and therefore, there is no uncertainty related to the system model. The nonlinear least squares estimator, on its discrete form, is responsible for minimizing a function of the squared residuals (Gelb, 2001). The batch least squares algorithm (Kuga, 2005) is then:

$$\hat{\mathbf{P}}_{\mathbf{i}} = (\bar{\mathbf{P}}_{\mathbf{0}}^{-1} + \mathbf{H}^{\mathbf{T}}\mathbf{R}^{-1}\mathbf{H})^{-1} \tag{15}$$

$$\delta\hat{\mathbf{x}}_{\mathbf{i}} = \hat{\mathbf{P}}_{\mathbf{i}}(\bar{\mathbf{P}}_{\mathbf{0}}^{-1}\delta\bar{\mathbf{x}}_{\mathbf{i-1}} + \mathbf{H}^{\mathbf{T}}\mathbf{R}^{-1}\delta\mathbf{y}), \tag{16}$$

where $\delta\mathbf{y}$ is the residual vector aligned along time, $\mathbf{H}$ is the Hessian matrix translated to the epoch, and $\delta\mathbf{x}$ is the state deviation along the iterations. Typically, the iterations continue until convergence is reached. The criterion used to terminate the algorithm consists of checking when the deviation becomes sufficiently small. The final solution to the state of each iteration will be:

$$\hat{\mathbf{x}}_{\mathbf{i}} = \hat{\mathbf{x}}_{\mathbf{i-1}} + \delta\hat{\mathbf{x}}_{\mathbf{i}}, \tag{17}$$

PLATFORMS

The first platform of this work was developed at INPE, at the end of 1980 decade with the aim of testing the nutation dampers of SCD2 Brazilian satellite. After 2010, many equipment were acquired to create a cold gas attitude control satellite simulator. The items are a PC/104 computer, an inertial unity, 8 gas valves and 2 air compressed tanks. A picture of the system can be seen in Fig. 1. The second platform of this work was acquired from Space Electronics. It is a 3-DoF
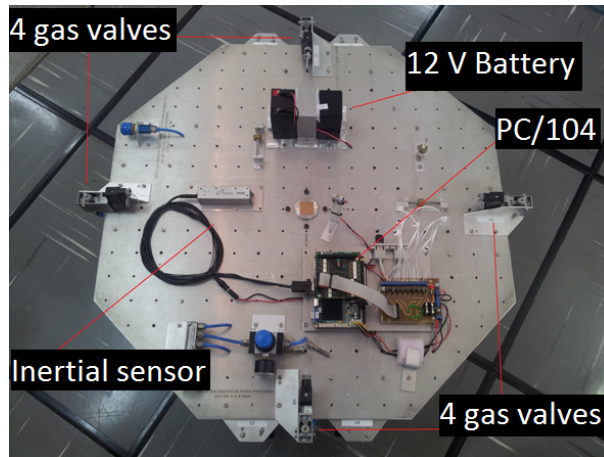

Figure 1 – INPE Air bearing table with cold gas actuators.

dumbbell air bearing with low friction. The equipment bought for this platform were acquired from Vectronic Aerospace and they are engineering models of real sensors and actuators used in different space missions. There are 3 fiber optic

gyroscopes, 3 reaction wheels, 3 magnetic coils, a GPS and a 3 axis magnetometer. All equipment have been integrated to a PCDH (Power Condition and Data Handling) computer capable of managing the power and data transmitted to and coming from each one. Additionally, this platform was placed in a room with retractile ceiling in order to allow star sensors reading at night. A picture of the system can be seen at Fig. 2.

Figure 2 – INPE dumbbell air bearing with Vectronic Aerospace equipment.

RESULTS

Figure 3 shows the experiment data obtained for the platform 1. On the left, it can be seen the Euler angles (rad) and, on the right, the angular velocities (rad/s) during 30 seconds. The experiment consists of spinning the platform around the Z axis. One can note that the angular velocity is decreasing and, therefore, there are dissipative forces acting on the air bearing. Figures 4 and 5 show the estimated mass properties (moments of inertia and center of gravity position) from
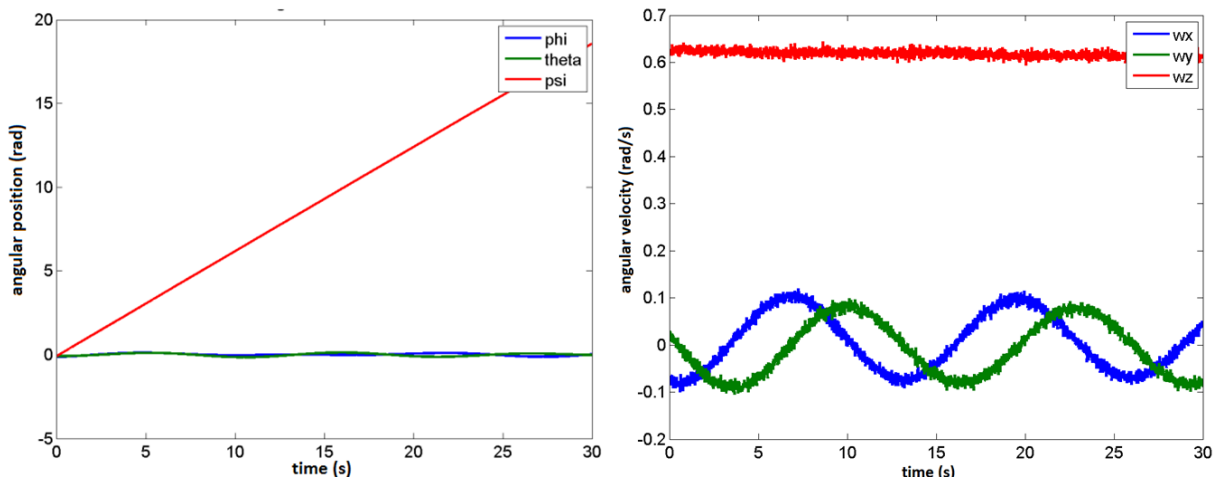
Figure 3 – Euler angles and angular velocities from the experiment of platform 1.

the platform 1 obtained with the extended Kalman filter. The median curve is the mean value of each parameter. Above and below curves show the estimated parameter plus or minus one standard deviation at the corresponding time. The final estimated values are shown at Tab. 1. The manual balancing proved effective, since that the obtained values for the center of gravity are on the order of a few tens of micrometers and the products of inertia are small enough, compared to the principal moments of inertia. The sample rate of the experiment of the platform 1 is 100 Hz.
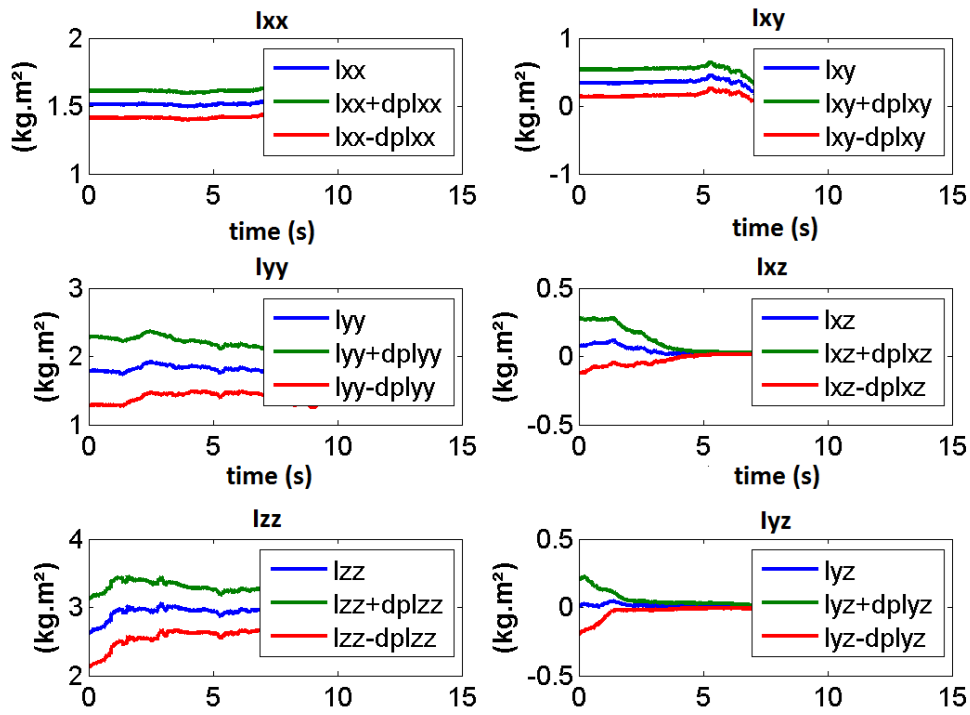
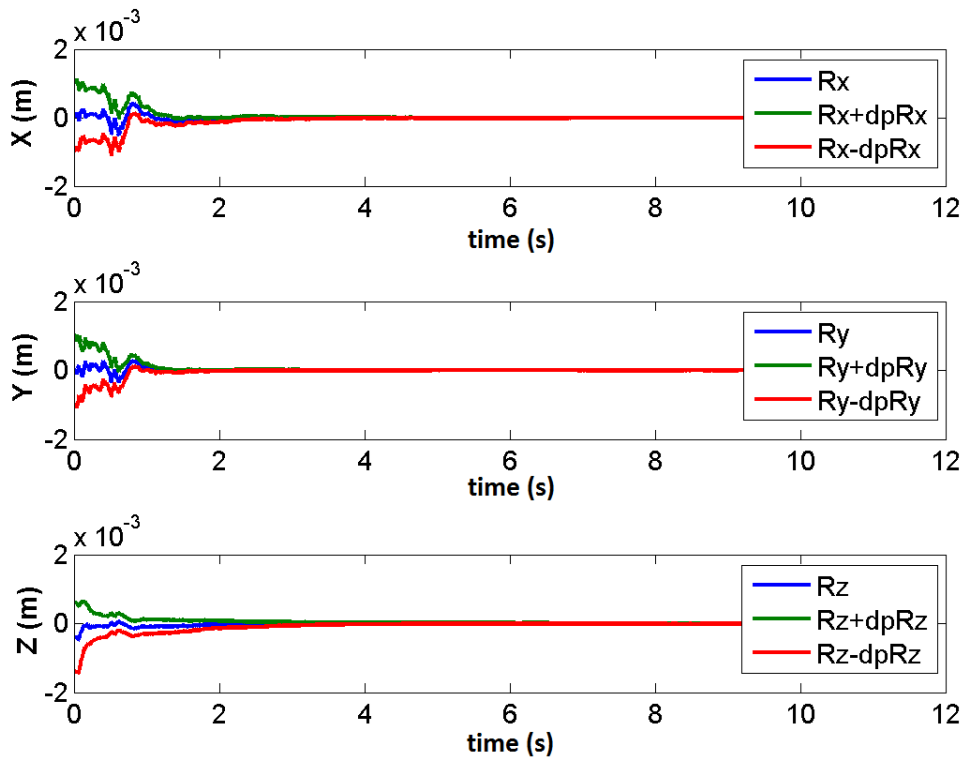Figure 4 – Moments of inertia of the platform 1.

Figure 5 – Gravity center of the platform 1.

Figure 6 shows the residues for the same experiment using the nonlinear least squares algorithm. Because it is an iterative algorithm, there are shown only the iteration numbers 1, 3 and 5. The zero mean noisy behavior proves the convergence of the algorithm. Table 2 shows the estimated values for the nonlinear least squares for the experiment at platform 1. As expected, we notice slight refinement of the results when compared to the extended Kalman filter. This refinement can be seen by the values of the covariance that are slightly lower than those obtained by the same experiment

Table 1 – Estimated values from the extended Kalman filter.

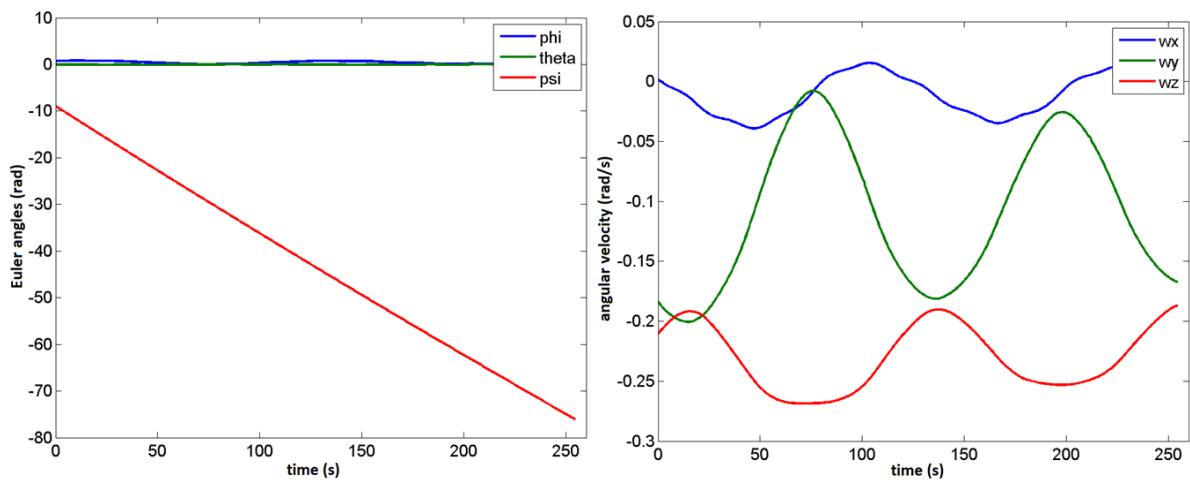| Variable	Values
Inertia Matrix ($km.m^2$)	$\mathbf{I} = \begin{bmatrix} 1.5231 & 0.0553 & 0.0198 \\ 0.0553 & 1.7131 & -0.0026 \\ 0.0198 & -0.0026 & 2.9016 \end{bmatrix}$
Gravity Center (m)	$\mathbf{R_{CG}} = \begin{bmatrix} -5.326 \times 10^{-6} \\ 4.911 \times 10^{-6} \\ -7.532 \times 10^{-6} \end{bmatrix}$
Covariance Matrix ($kg*m^2)^2$	$\mathbf{P(I)} = \begin{bmatrix} 0.0415 & 0.0128 & 0.0027 \\ 0.0128 & 0.0719 & 0.0022 \\ 0.0027 & 0.0022 & 0.0690 \end{bmatrix}$
Covariance Matrix (m^2)	$\mathbf{P(R_{CG})} = \begin{bmatrix} 2.95 \times 10^{-9} \\ 2.74 \times 10^{-9} \\ 7.19 \times 10^{-8} \end{bmatrix}$
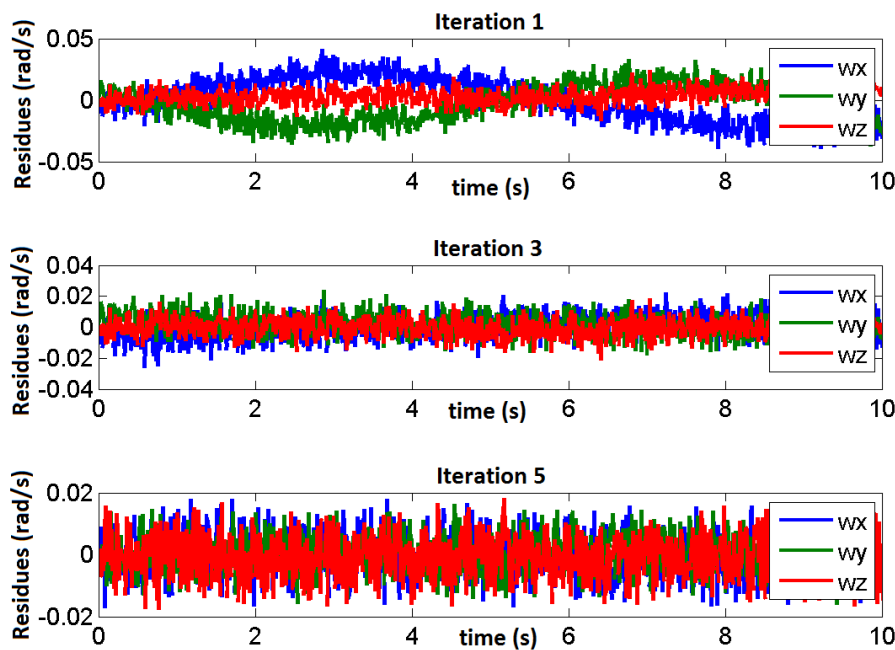
Figure 6 – Angular velocity residues from nonlinear least squares algorithm for platform 1.

with the extended Kalman filter. Figure 7 shows the experiment data obtained for the angular positions and angular velocities from the platform 2 during 250 seconds. The experiment also consists of spinning the platform around the Z axis. Once again, the amplitude of the sinusoidal curves of the angular velocities is decreasing over time, indicating that there are also dissipative forces acting on this platform. Figures 8 and 9 show the estimated mass properties from the platform 2 obtained with the extended Kalman filter. The final estimated values are shown at Tab. 3. The manual balancing also proved effectiveness, since that the obtained values for the center of gravity are also on the order of a few micrometers. On the other hand, the products of inertia need to be reduced to decrease the nonlinear characteristic of the movement. The obtained values for the products of inertia represent 10 percent of the moment of inertia I_{xx}. The largest number of cables, connectors and equipment difficult balancing the inertia matrix of the dumbbell air bearing table. The sample rate of this experiment is 2 Hz, a limitation of the onboard computer of this platform. For this reason, the time of the experiment is much larger than the experiments at platform 1. Figure 10 shows the residues for the same experiment using the nonlinear least squares algorithm for platform 2. Because it is an iterative algorithm, there is also shown only the iteration numbers 1, 3 and 5. Despite the residues decreasing considerably, there is still a sinusoidal pattern at the residues. It is believed that this fact is due to the low sampling rate of the experiment. Table 4 shows the estimated values of the mass properties with the nonlinear least squares algorithm for platform 2. As expected, it was noticed once more a slight refinement of the results when compared to the extended Kalman filter. This refinement can be seen by the values of the covariance matrix that are slightly lower than those obtained by the same experiment with the extended Kalman filter.

Table 2 – Estimated values from the nonlinear least squares algorithm for the experiment at platform 1.

Variable	Values	
Matrix of Inertia $(km.m^2)$	$\mathbf{I} = \begin{bmatrix} 1.5941 & 0.0912 & 0.0106 \\ 0.0912 & 1.6992 & 0.0186 \\ 0.0106 & 0.0186 & 2.9040 \end{bmatrix}$	
Gravity Center (m)	$\mathbf{R_{CG}} = \begin{bmatrix} -3.080 \times 10^{-5} \\ 4.992 \times 10^{-5} \\ -4.075 \times 10^{-5} \end{bmatrix}$	
Covariance Matrix $(kg * m^2)^2$	$\mathbf{P(I)} = \begin{bmatrix} 0.0401 & 0.0319 & 0.0060 \\ 0.0319 & 0.0597 & 0.0059 \\ 0.0060 & 0.0059 & 0.0746 \end{bmatrix}$	
Covariance Matrix (m^2)	$\mathbf{P(R_{CG})} = \begin{bmatrix} 1.909 \times 10^{-9} \\ 1.648 \times 10^{-9} \\ 6.740 \times 10^{-7} \end{bmatrix}$	

Figure 7 – Euler angles and angular velocities from the experiment of platform 2.

Table 3 – Estimated values from the nonlinear least squares algorithm for the experiment at platform 2.

Variable	Values	
Inertia Matrix $(km.m^2)$	$\mathbf{I} = \begin{bmatrix} 3.0948 & 0.3832 & 0.2712 \\ 0.3832 & 12.1409 & -0.0167 \\ 0.2712 & -0.0167 & 12.2756 \end{bmatrix}$	
Gravity Center (m)	$\mathbf{R_{CG}} = \begin{bmatrix} +0.345 \times 10^{-6} \\ -7.504 \times 10^{-6} \\ -4.906 \times 10^{-6} \end{bmatrix}$	
Covariance Matrix $(kg * m^2)^2$	$\mathbf{P(I)} = \begin{bmatrix} 0.07362 & 0.00298 & 0.00982 \\ 0.00298 & 1.26191 & 0.00043 \\ 0.00982 & 0.00043 & 1.25906 \end{bmatrix}$	
Covariance Matrix (m^2)	$\mathbf{P(R_{CG})} = \begin{bmatrix} 1.003 \times 10^{-10} \\ 6.489 \times 10^{-12} \\ 2.211 \times 10^{-11} \end{bmatrix}$	

Kinetic Energy Considerations

Other estimation experiments were also performed on both platforms during this work (Oliveira, 2014). The graphs of the kinetic energy shown below are comparisons of two experiments performed on each of the platforms.

The kinetic energy was calculated using the estimated values of the least squares algorithm for both platforms in order to measure the amount of energy dissipated during the experiments. Figure 11 shows the graph of kinetic energy for the
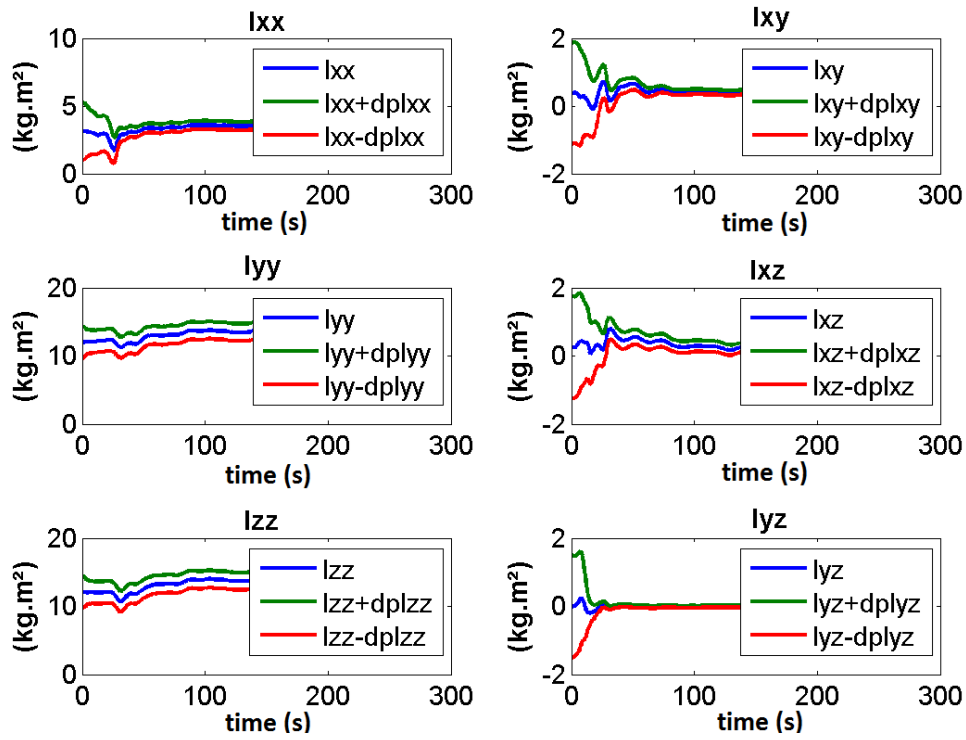
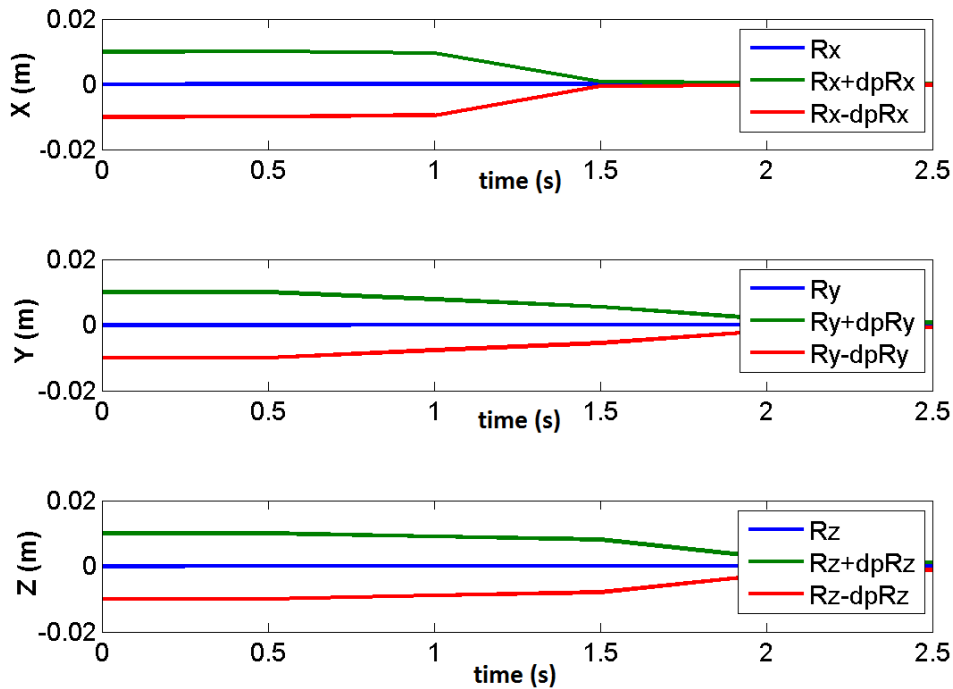**Figure 8 – Estimated moments of inertia from extended Kalman filter from platform 2.**

Figure 9 – Estimated center of gravity position from the extended Kalman filter of platform 2.

platform 1. It can be seen that, over 30 seconds of the experiments on platform 1, the kinetic energy of the experiment 1 decreased 18.8%, caused by a torque of about 7.1 mNm. In experiment 2, the kinetic energy decreased by around 5%, caused by a torque of approximately 2.8 mNm. This fact is quite harmful to the least-squares algorithm that does not include uncertainties in the dynamic model of the system. It is observed that much of this energy loss can be modeled by a friction torque of viscous nature and, therefore, proportional to the angular velocity of the platform. This can be seen by the ratio between friction torque and the magnitude of the angular velocity for the Z axis, in experiment 1 is 0.2268 rad/mNm.s and in experiment 2 is 0.2349 rad/mNm.s. It can be deduced the fact that for low angular velocities,
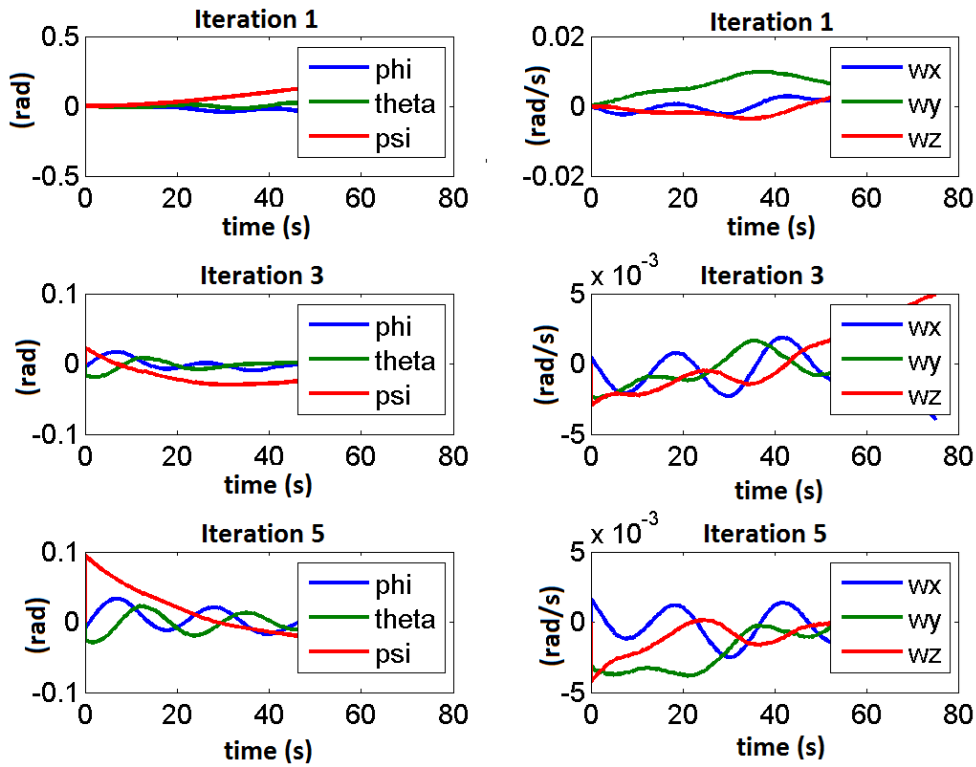
Figure 10 – Euler angles and angular velocities residues from the nonlinear least squares algorithm - platform 2.

Table 4 – Estimated values from the nonlinear least squares algorithm for the experiment at platform 2.

Variable		Values
Inertia Matrix ($km.m^2$)	$\mathbf{I} =$	$\begin{bmatrix} 3.1241 & 0.3780 & 0.2550 \\ 0.3780 & 11.9444 & -0.0259 \\ 0.2550 & -0.0259 & 12.1381 \end{bmatrix}$
Gravity Center (m)	$\mathbf{R_{CG}} =$	$\begin{bmatrix} -1,05851 \times 10^{-5} \\ -9,37020 \times 10^{-5} \\ -2,09563 \times 10^{-5} \end{bmatrix}$
Covariance Matrix ($(kg * m^2)^2$)	$\mathbf{P(I)} =$	$\begin{bmatrix} 0.06592 & 0.00202 & 0.00753 \\ 0.00202 & 1.21493 & 0.00041 \\ 0.00753 & 0.00041 & 1.17932 \end{bmatrix}$
Covariance Matrix (m^2)	$\mathbf{P(R_{CG})} =$	$\begin{bmatrix} 9.1760 \times 10^{-9} \\ 3.5682 \times 10^{-9} \\ 4.8001 \times 10^{-9} \end{bmatrix}$

the platform better reproduces the space environment, since the friction will be very close to zero. Figure 12 shows the kinetic energy results for the platform 2. It can be seen that during the first 100 seconds of each experiment, the kinetic energy decreased by 9% in experiment 1 caused by a torque of 1.5 mNm and approximately 6% in experiment 2, caused by a torque of approximately 0.97 mNm. Again, this fact is quite harmful to the least-squares algorithm that does not include uncertainties in the dynamic model of the system. It can be deduced from these results that much of the friction has also viscous nature and, therefore, is proportional to the angular velocity of platform. This can be seen by the ratio between friction torque and the magnitude of the angular velocity for the Z axis, in experiment 1 is 0.1791 rad/mNm and in experiment 2 is 0.1521 rad/mNm. We deduce from such fact that, for low angular speed, the dumbbell air bearing platform also reproduces the space environment, since the friction will be nearing zero.

Control experiments for validation

For both platforms, we develop a PD control algorithm using the moments of inertia obtained with nonlinear least square estimators. For platform 1, we add a dead zone with 1.5 degrees in order to preserve the electronic actuators of gas valves. The same is not necessary for the platform 2 since the actuators are reaction wheels. Two simplifying assumptions
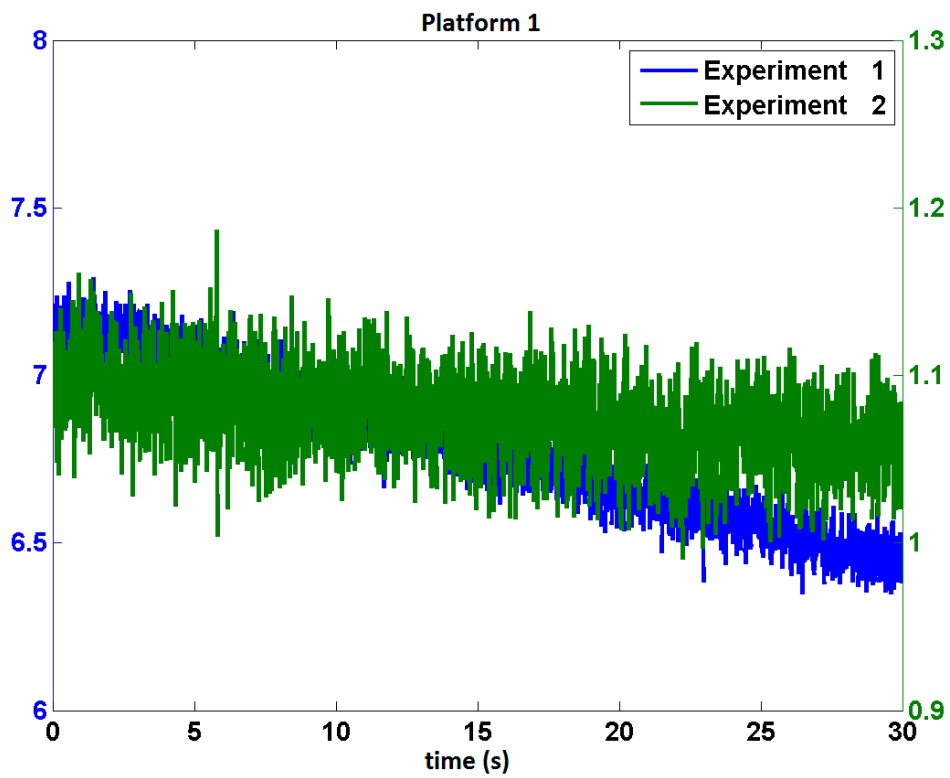
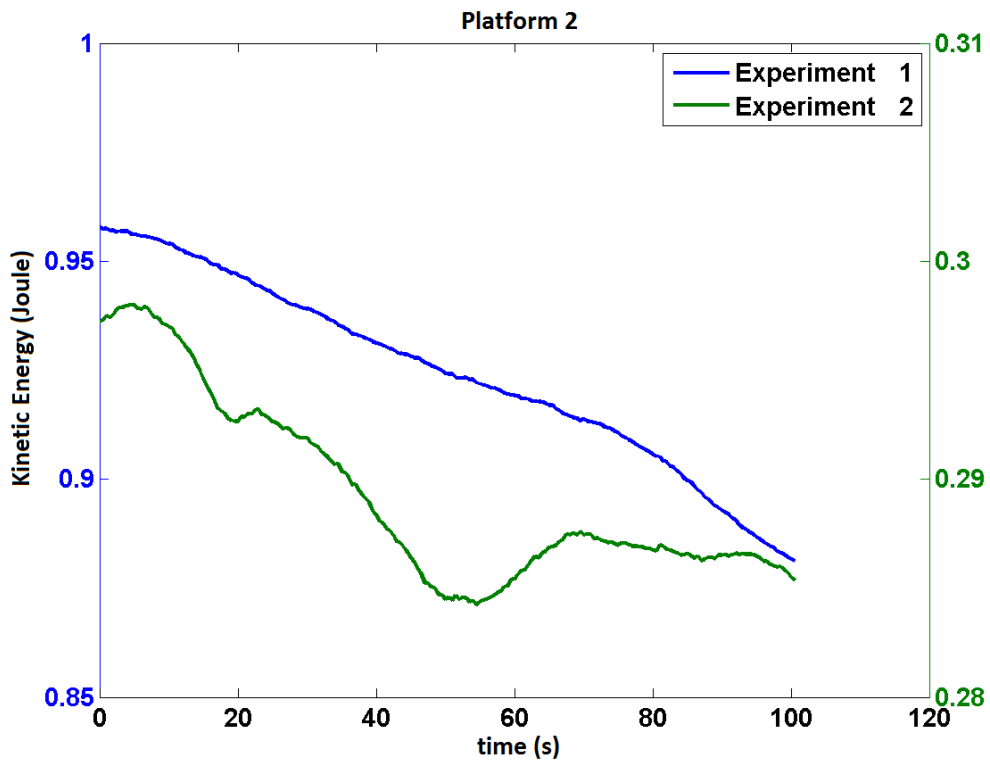**Figure 11 – Kinetic energy for two different experiments with the air bearing platform 1.**

Figure 12 – Kinetic energy for two different experiments with the dumbbell air bearing platform 2.

were made in order to approximate the nonlinear dynamics of rotation to a linear and uncoupled system.

The first one was to consider negligible the products of inertia, and so the inertia matrix became diagonal. The second

was to admit that the body rotation rate is very small. These two assumptions together greatly reduce the nonlinear portion of the system and makes uncoupling between body axes possible. Figures 13 and 14 show the block diagrams for both control experiments. For platform 1, the control system was designed so that the response to the step input has
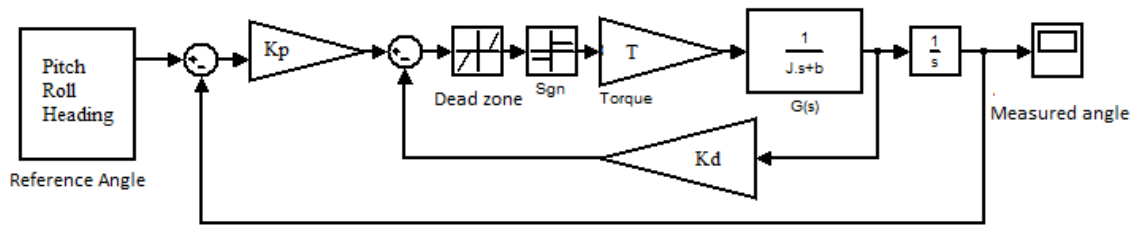

Figure 13 – PD control algorithm for platform 1 with gas valves as actuators. The coefficient b represent a friction torque.
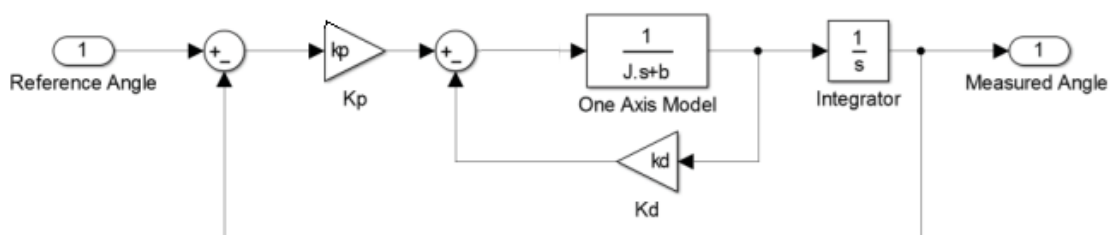

Figure 14 – PD control algorithm for platform 2 with reaction wheels as actuators. The coefficient b represent a friction torque.

no overshoot, with 20 seconds of settling time. The gains used in the controller are $kp = 0.2$ and $kd = 1.2$. Despite being designed to only the Z-axis of this platform, the same gains were also used in the other axes. Figure 15 shows the Euler angles for this experiment during time. It can be seen that there was no overshoot in the response of the Z axis, as designed. However, the settling time was 27 seconds. This fact is expected since the addition of the dead zone in the system degrades the designed response, increasing the settling time. On the other hand, for platform 2, the controller
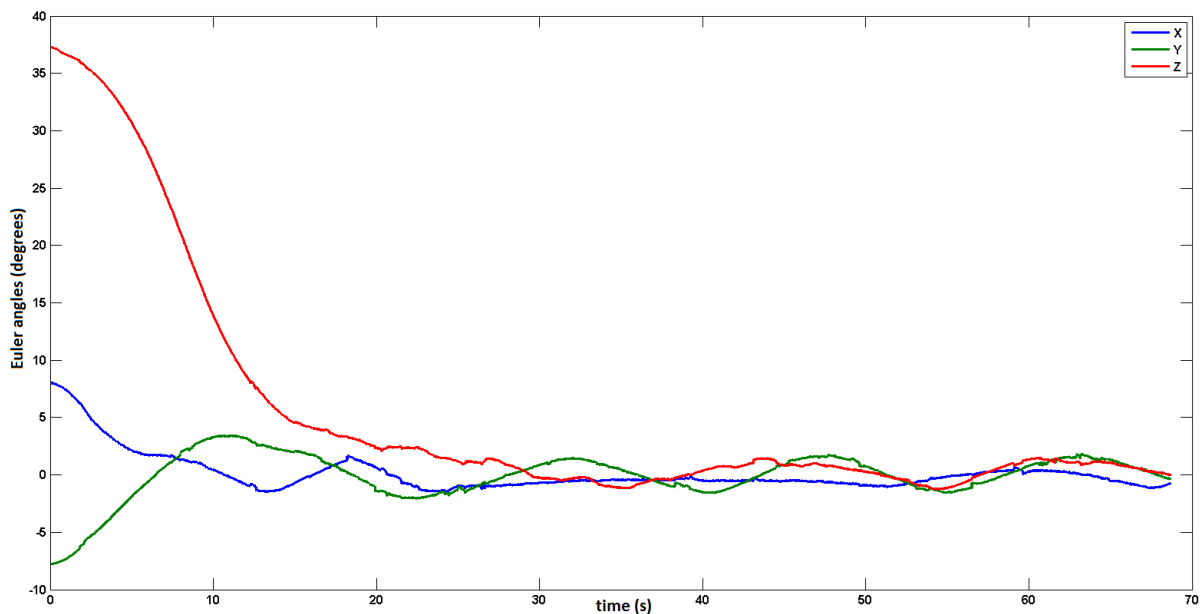

Figure 15 – Euler angles of the control experiment of platform 1.

design was done separately for each axis. The gains for the 3-axes controller were computed so as to give a response with

a 10% overshoot and settling time of 100 seconds. The proportional gains are, for x,y and z axes: 0.01573, 0.05751 and 0.05830, while derivative gains are 0.27388, 1.00404 and 1.01772. Platform 2 was commanded to perform a 180 degrees rotation about z-axis. Figure 16 shows the Euler angles for this experiment during time, while Fig. 17 shows the applied reaction wheel torque during time. It is remarkable that the torque saturates quickly, as soon as the control begins to maneuver the platform. Probably due to saturation of the reaction wheel torque, the overshoot was slightly reduced when compared to the designed values. In fact, the measured overshoot in z-axis was only 7.5%. The measured settling time of 101.6 s, on the other hand, was close to the designed one. However, it was expected a bigger time due to the torque saturation.
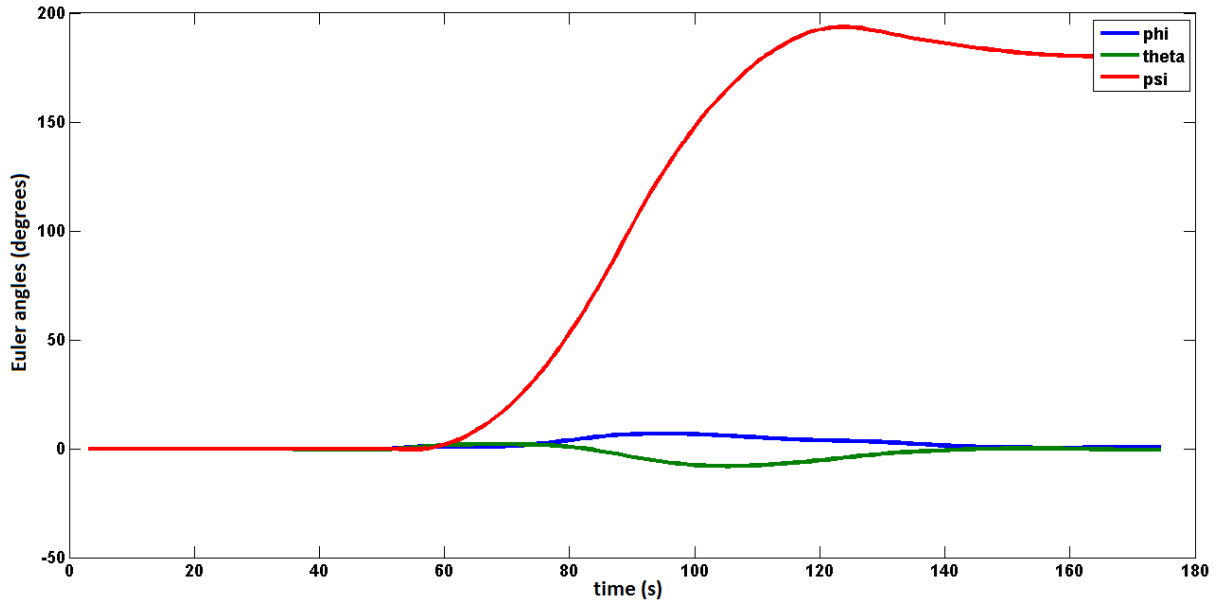

Figure 16 – PD control algorithm for platform 2 with reaction wheels as actuators. The coefficient b represent a friction torque.
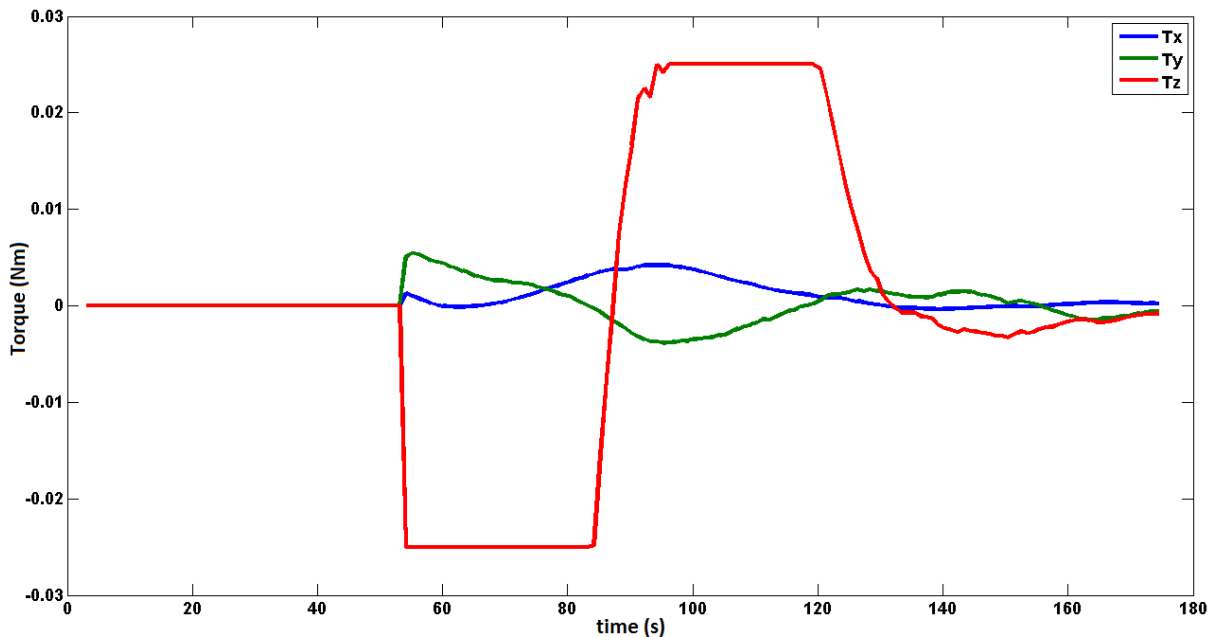

Figure 17 – Applied reaction wheel torque. Saturation limits the torque to 0.025 mNm.

CONCLUSIONS

This study aimed to demonstrate the use of estimation algorithms to obtain experimentally the mass properties of aerostatic platforms for use in space applications in order to develop a satellite simulator for attitude control subsystems testing. Several sensors, actuators and embedded electronics were integrated into both platforms in order to create minimum torque environment, similar to a satellite drifting in space. In both platforms, the estimation algorithms have achieved satisfactory mass properties values that could be validated by the control experiments.

The control algorithm proposed for the platform 1 used the estimated inertia values for the calculation of gains and satisfactorily controlled the attitude of the table on three axes, stabilizing it in the desired position. Small errors in the estimation process may have happened. However, the controller compensated for these errors (which may also be considered as disturbances), since the profile of the response curve was consistent with the designed controller.

The control experiment in the platform 2 was also quite satisfying and succeeded in controlling the attitude of the table in three axes, stabilizing it in the desired position. The use of reaction wheels enables fine adjustment of the attitude of the platform, allowing the future development of autonomous control of a 3-axis attitude for Brazilian satellites. The response of the platform to the designed controller is consistent with the designed one. As a general rule, the kinetic energy of the two platforms, in all tests decreased during the estimation process. In the case of the platform 2, which has higher quality of both the equipment and platform, the number of non-rigid cables, washers and screws certainly influenced to reduce energy. It is believed, however, that the main source of friction in the two bearings is caused by friction with air, as shown in the kinectic energy considerations topic. It should not be forgotten that the internal torques (rigid and non-flexible) only reduce the energy associated with nutation. The angular momentum vector is not changed by internal torques. It is only expected that the coning motion decrease in this case (Hugues, 1986; Wertz, 1978).

Finally, it is worth to mention that this work is the first initiative of a fully instrumented 3-axis satellite attitude controller performed in Brazil, and surely the test platforms (air bearing tables) shall be invaluable for attitude control development and helpful to future Brazilian space missions.

ACKNOWLEDGMENTS

REFERENCES

Aguirre, L. A., 2007, Introdução a identificação de sistemas, 3rd Ed., Minas Gerais, Brazil, 730 p.

Gelb, A., 1974, Applied optimal estimation, MA, USA: Ed. MIT Press, 384 p.

Hughes, P. C., 1986, Spacecraft attitude dynamics, NY, USA: Ed. Dover Publications, 570 p.

Kuga, H. K., 2005, Noções práticas de técnicas de estimação, [S.l.]: Notas de Aula: Otimização em sistemas dinâmicos II, INPE, São José dos Campos, Brazil.

Lefferts, E. J.; Markley, F. L.; Shuster, M. D., 1962, Kalman filtering for spacecraft attitude estimation, Journal of guidance, control, and dynamics, New York, USA, v. 5, n. 5, pp. 417-429.

Maybeck, P. S., 1979, Stochastic models, estimation, and control, New York, USA: Ed. New York: Academic Press, 423p.

Oliveira, A. M., 2014, "Estimação das características de massa de mancais aerostáticos para aplicações espaciais". Dissertação (Mestrado em Mecânica Espacial e Controle (Instituto Nacional de Pesquisas Espaciais), São José dos Campos, 104p.

Schwartz, J. L., Peck, M. A., Hall, C. D., 2003, "Historical Review of Air-Bearing Spacecraft Simulators", Journal of Guidance, Control, and Dynamics, Vol. 26, No. 4, pp. 513-522.

Wertz, J. R., 1978, Spacecraft attitude determination and control, Dordrecht, The Netherlands: Ed. Kluwer Academic Publishers, 860 p.

RESPONSIBILITY NOTICE

The author(s) is (are) the only responsible for the printed material included in this paper.